Supporting Information: Interfacial Structure and Tension of Polyelectrolyte Complex Coacervates

Pengfei Zhang*,† and Zhen-Gang Wang*,‡

†*State Key Laboratory for Modification of Chemical Fibers and Polymer Materials, Center for Advanced Low-Dimension Materials, College of Material Science and Engineering, Donghua University, Shanghai 201620, China*

‡*Division of Chemistry and Chemical Engineering, California Institute of Technology, Pasadena, CA 91125, United States*

E-mail: pfzhangphy@dhu.edu.cn; zgw@caltech.edu

S1. Chemical potential and osmotic pressure

From the bulk free energy density f_b given by Eq. (10) of the main text, we calculate the chemical potential for polycation and polyanion respectively as

$$\begin{aligned}\frac{\mu_{b,p+}}{k_BT} &= \frac{1+\ln\phi_{p+}}{N_{p+}} - \ln\left(1-\sum_{i=p\pm,\pm}\phi_i\right) - 1 + \left(\frac{1}{N_{p+}}-1\right)\left[\frac{2\pi\phi_{p+}z_{p+}^4\left(l_B/\sigma\right)^2}{(1+\kappa\sigma)^2(\kappa\sigma)} - \frac{z_{p+}^2 l_B/\sigma}{1+\kappa\sigma}\right] \\ &\quad + \left(\frac{1}{N_{p-}}-1\right)\frac{2\pi\phi_{p-}z_{p+}^2 z_{p-}^2\left(l_B/\sigma\right)^2}{(1+\kappa\sigma)^2(\kappa\sigma)} - \frac{z_{p+}^2\kappa l_B}{2(1+\kappa\sigma)} \end{aligned} \tag{S1}$$

and

$$\frac{\mu_{b,p-}}{k_BT} = \frac{1+\ln\phi_{p-}}{N_{p-}} - \ln\left(1-\sum_{i=p\pm,\pm}\phi_i\right) - 1 + \left(\frac{1}{N_{p-}}-1\right)\left[\frac{2\pi\phi_{p-}z_{p-}^4\left(l_B/\sigma\right)^2}{(1+\kappa\sigma)^2(\kappa\sigma)} - \frac{z_{p-}^2 l_B/\sigma}{1+\kappa\sigma}\right] + \left(\frac{1}{N_{p+}}-1\right)\frac{2\pi\phi_{p+}z_{p+}^2 z_{p-}^2\left(l_B/\sigma\right)^2}{(1+\kappa\sigma)^2(\kappa\sigma)} - \frac{z_{p-}^2\kappa l_B}{2(1+\kappa\sigma)}. \quad \text{(S2)}$$

Likewise, the chemical potential of cation and anion is

$$\frac{\mu_{b,j}}{k_BT} = \ln\phi_j - \ln\left(1-\sum_{i=p\pm,\pm}\phi_i\right) + \left(\frac{1}{N_{p+}}-1\right)\frac{2\pi\phi_{p+}z_{p+}^2 z_j^2\left(l_B/\sigma\right)^2}{(1+\kappa\sigma)^2(\kappa\sigma)} + \left(\frac{1}{N_{p-}}-1\right)\frac{2\pi\phi_{p-}z_{p-}^2 z_j^2\left(l_B/\sigma\right)^2}{(1+\kappa\sigma)^2(\kappa\sigma)} - \frac{z_j^2\kappa l_B}{2(1+\kappa\sigma)} \quad \text{(S3)}$$

with $j = +$ and $-$ respectively.

With f_b and μ_i, we obtain the osmotic pressure as

$$\begin{aligned}\frac{\Pi_b v}{k_BT} &= \frac{1}{k_BT}\left[-vf_b + \sum_{i=p\pm,\pm}\mu_{b,i}\phi_i - vf_b(\{\phi_i=0\})\right] \\ &= \sum_{i=p\pm,\pm}\frac{\phi_i}{N_i} - \ln\left(1-\sum_{i=p\pm,\pm}\phi_i\right) - \sum_{i=p\pm,\pm}\phi_i + \frac{1}{4\pi}\left[\ln(1+\kappa\sigma) - \frac{2\kappa\sigma+(\kappa\sigma)^2}{2(1+\kappa\sigma)}\right] \\ &\quad + \frac{\kappa l_B}{2(1+\kappa\sigma)^2}\left[\left(N_{p+}^{-1}-1\right)\phi_{p+}z_{p+}^2 + (N_{p-}^{-1}-1)\phi_{p-}z_{p-}^2\right]. \quad \text{(S4)}\end{aligned}$$

S2. Bulk concentration of the different species and the Galvani potential at coexistence

Here we present the effects of the three controlling parameters – the added-salt concentration $\phi_{s,0}$, the initial polymer concentration $\phi_{p,0}$, and the asymmetry factor r, on the bulk coexistence properties, including the concentrations of all the species in the two coexisting phases $\phi_i^{\rm I}$ and $\phi_i^{\rm II}$ with $i = p+, p-, +, -$, and the Galvani potential Ψ_G, for the concentration-asymmetric complex coacervation, using the theory developed in the main text. These bulk quantities serve as the boundary conditions when calculating the interfacial properties of the asymmetric coacervates at a given parameter set. The bulk properties reported here are qualitatively similar to those examined in our previous work.[S1]

S2.1. Effect of added-salt concentration $\phi_{s,0}$

We first examine the effect of added-salt concentration $\phi_{s,0}$. Taking the system with $\phi_{p,0} = 0.02$ and $r = 1/3$ as an example, in Fig. S1 we show the concentration of all the species in the supernatant and coacervate phases, and the Galvani potential. The value of $r = 1/3$ means that the volume of polycation solution is twice that of polyanion solution, so that in the mixture polycation is the major polyion species while polyanion is the minor species. All curves in the figures terminate once $\phi_{s,0}$ is larger than the phase boundary value $\phi_{s,0}^*$ where the solution enters a single homogeneous phase.

From Fig. S1(a), we see that, except in the region very close to $\phi_{s,0}$, both polyion concentrations in the supernatant phase, $\phi_{p+}^{\rm I}$ and $\phi_{p-}^{\rm I}$, remain nearly unchanged. While $\phi_{p-}^{\rm I}$ is rather small and is very close to 0, $\phi_{p+}^{\rm I}$ is moderately finite. On the other hand, Fig. S1(b) shows that the concentration of both polyions in the coacervate phase $\phi_{p+,p-}^{\rm II}$ decreases monotonically with $\phi_{s,0}$. Note that $\phi_{p+}^{\rm II}$ is slightly larger than $\phi_{p-}^{\rm II}$ for all $\phi_{s,0}$, indicating that a slight excess of polycation over polyanion in the coacervate. Therefore, there is a weak charge

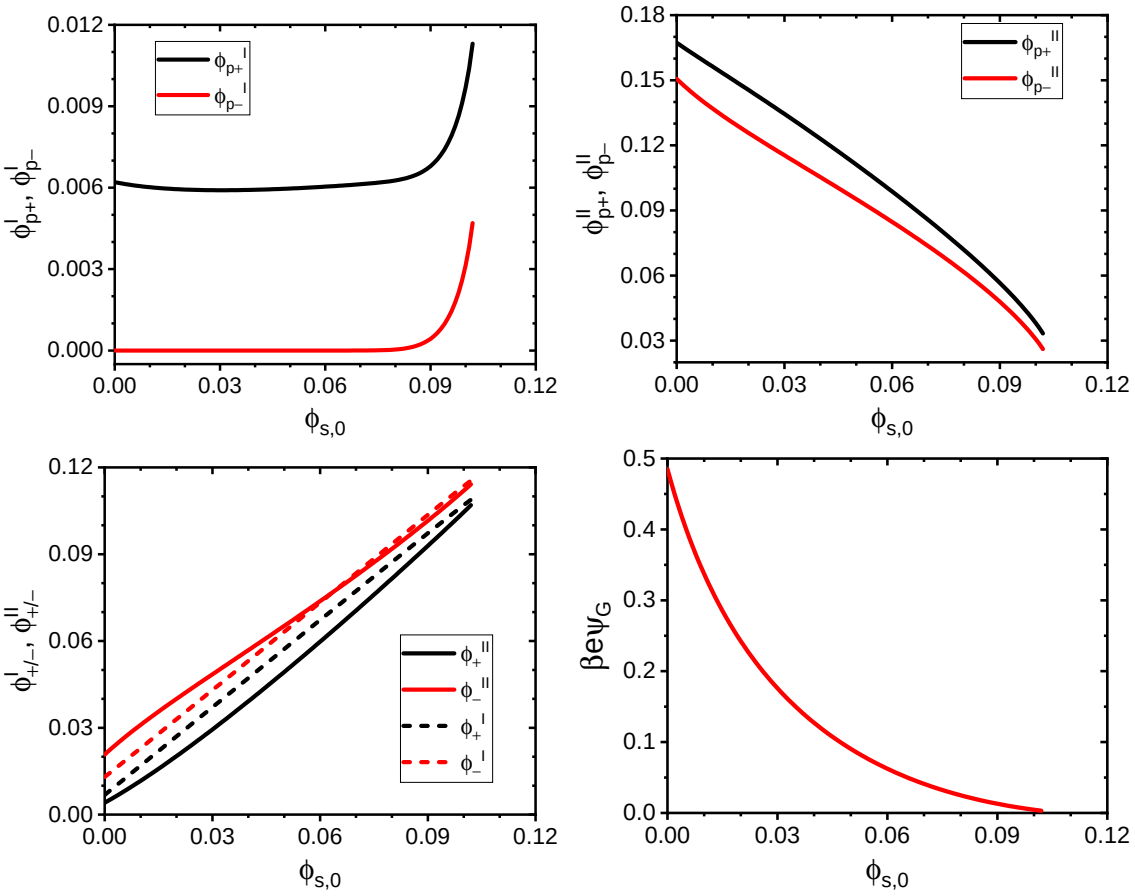

Figure S1: Polycation and polyanion concentration (a) in the supernatant phase $\phi^{\mathrm{I}}_{p\pm}$, and (b) in the coacervate phase $\phi^{\mathrm{II}}_{p\pm}$, and (c) cation and anion concentration in both the supernatant and coacervate phases $\phi^{\mathrm{I/II}}_{\pm}$ as a function of the added-salt concentration $\phi_{s,0}$ for the system with $r = 1/3$ and $\phi_{p,0} = 0.02$. Panel (d) denotes the Galvani potential as a function of $\phi_{s,0}$.

imbalance between polycation and polyanion in the coacervate phase; however, the charge neutrality is still satisfied by salt ions.

In Fig. S1(c), we show both cation and anion concentrations in the supernatant and coacervate phases $\phi^{\mathrm{I}}_{\pm}$ and $\phi^{\mathrm{II}}_{\pm}$, as a function of $\phi_{s,0}$. In general, both $\phi^{\mathrm{I}}_{\pm}$ and $\phi^{\mathrm{II}}_{\pm}$ increase with $\phi_{s,0}$. Moreover, while $\phi^{\mathrm{I}}_{+} > \phi^{\mathrm{II}}_{+}$ for all $\phi_{s,0}$, we find $\phi^{\mathrm{I}}_{-} > \phi^{\mathrm{II}}_{-}$ at small $\phi_{s,0}$ and $\phi^{\mathrm{I}}_{-} < \phi^{\mathrm{II}}_{-}$ at large $\phi_{s,0}$. Finally, Fig. S1(d) shows that the Galvani potential Ψ_G, i.e., the electrostatic potential of the coacervate phase relative to that of the supernatant phase, decreases monotonically.

S2.2 Effect of initial polymer concentration $\phi_{p,0}$

Next, we present the dependence of the bulk phase behaviors on the initial polymer concentration $\phi_{p,0}$ for a concentration-asymmetric coacervation. Taking the system with $r = 1/3$ and $\phi_{s,0} = 0$ as an example, in Fig. S2(a) we show both polyion concentrations in the supernatant phase $\phi^{\mathrm{I}}_{p\pm}$ as a function of $\phi_{p,0}$. While ϕ^{I}_{p-} is rather small and nearly independent of $\phi_{p,0}$, ϕ^{I}_{p+} increases approximately linearly with $\phi_{p,0}$. On the other hand, Fig. S2(b) shows that, both polyion concentrations in the coacervate phase $\phi^{\mathrm{II}}_{p\pm}$ decreases monotonically with $\phi_{p,0}$. Again, $\phi^{\mathrm{II}}_{p+} > \phi^{\mathrm{II}}_{p-}$ and the difference between them increases with $\phi_{p,0}$, indicating the charge imbalance between polycation and polyanion increases slightly with increasing $\phi_{p,0}$.

Moreover, in Fig. S2(c), we show both cation and anion concentrations in the supernatant and coacervate phases, $\phi^{\mathrm{I}}_{+/-}$ and $\phi^{\mathrm{II}}_{+/-}$, as a function of $\phi_{p,0}$. While $\phi^{\mathrm{I}}_{+} > \phi^{\mathrm{II}}_{+}$ for all $\phi_{p,0}$, we see that $\phi^{\mathrm{I}}_{-} < \phi^{\mathrm{II}}_{-}$ at small $\phi_{p,0}$ and $\phi^{\mathrm{I}}_{-} > \phi^{\mathrm{II}}_{-}$ at large $\phi_{p,0}$. Finally, Fig. S2(d) shows that the Galvani potential Ψ_G decreases monotonically with $\phi_{p,0}$.

S2.3. Effect of asymmetry factor r

We further examine the effect of the asymmetric factor r on the phase behaviors of a concentration-asymmetric complex coacervation. Taking the system with $\phi_{p,0} = 0.02$ and $\phi_{s,0} = 0$ as an example, in Fig. S3 we show the concentrations of all the species and the Galvani potential as a function of r. First, in Fig. S3(a) we show the concentrations of both polyions in the supernatant phase ϕ^{I}_{p+} and ϕ^{I}_{p-}. While ϕ^{I}_{p-} is always rather small and very close to 0, we observe two r regimes for ϕ^{I}_{p+}. When $r \lesssim 0.05$, ϕ^{I}_{p+} is also rather small; when $r \gtrsim 0.05$, ϕ^{I}_{p+} takes moderately finite values and increases approximately linearly with r. On the other hand, in Fig. S3(b) we show both polyion concentration in the coacervate phase ϕ^{II}_{p+} and ϕ^{II}_{p-}. Generally, ϕ^{II}_{p-} decreases monotonically with r, but ϕ^{II}_{p+} varies only slightly with r. The two r regimes in ϕ^{II}_{p+} can also be clearly observed in ϕ^{II}_{p-}.

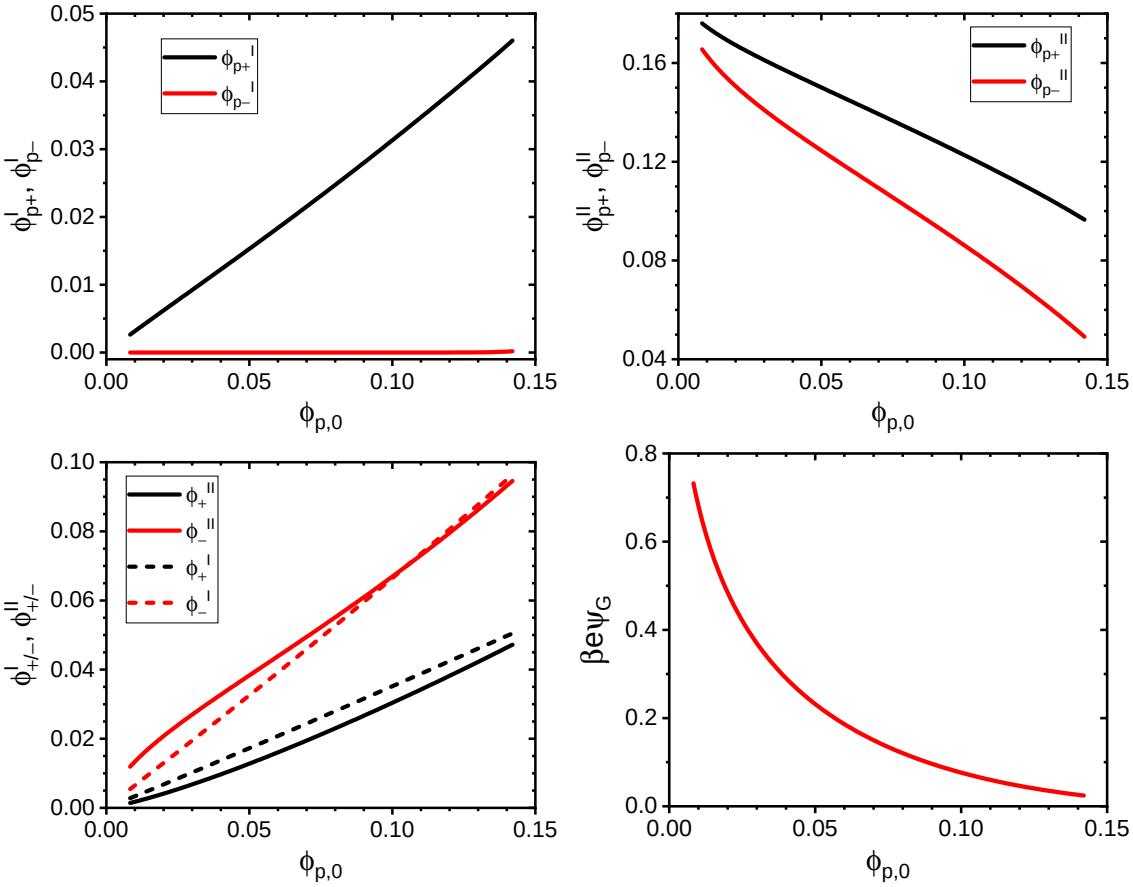

Figure S2: Polycation and polyanion concentration (a) in the supernatant phase $\phi^{\mathrm{I}}_{p\pm}$, and (b) in the coacervate phase $\phi^{\mathrm{II}}_{p\pm}$, and (c) cation and anion concentration in both the supernatant and coacervate phases $\phi^{\mathrm{I/II}}_{\pm}$ as a function of the initial polymer concentration $\phi_{p,0}$ for the system with $r = 1/3$ and $\phi_{s,0} = 0$. Panel (d) denotes the Galvani potential as a function of $\phi_{p,0}$.

In Fig. S3 (c), we further show the concentration of cation and anion in the supernatant and coacervate phases $\phi^{\mathrm{I}}_{+/-}$ and $\phi^{\mathrm{II}}_{+/-}$. We also observe the two distinct r regimes in which $\phi^{\mathrm{I}}_{+/-}$ and $\phi^{\mathrm{II}}_{+/-}$ behave differently. When $r \lesssim 0.05$, both ϕ^{I}_{+} and ϕ^{I}_{-} remain nearly unchanged, but ϕ^{II}_{+} decreases monotonically and ϕ^{II}_{+} increases monotonically. When $r \gtrsim 0.05$, both ϕ^{I}_{+} and ϕ^{II}_{+} decreases monotonically while ϕ^{I}_{-} and ϕ^{II}_{-} increase monotonically. The absolute value of the slope of $\phi^{\mathrm{II}}_{+/-}$ at large r, however, is smaller than that at small r. Further, for most cases, $\phi^{\mathrm{I}}_{+} < \phi^{\mathrm{II}}_{+}$ but $\phi^{\mathrm{I}}_{-} > \phi^{\mathrm{II}}_{-}$. Finally, Fig. S3(d) shows that the Galvani potential Ψ_G exhibit a maximum around $r \approx 0.05$. The physical mechanism underlying these two r regimes has been discussed in our previous work,[S1] and thus will be not repeated here.

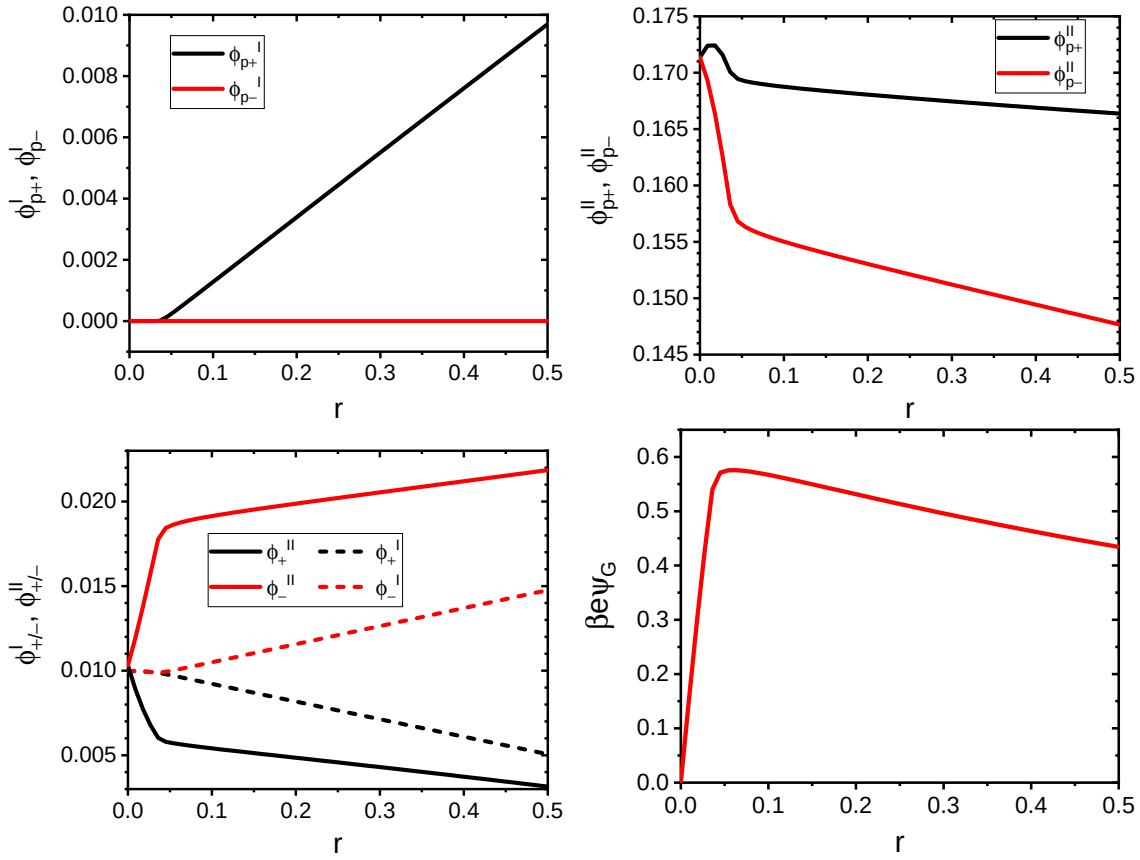

Figure S3: Polycation and polyanion concentration (a) in the supernatant phase $\phi^{\mathrm{I}}_{p\pm}$, and (b) in the coacervate phase $\phi^{\mathrm{II}}_{p\pm}$, and (c) cation and anion concentration in both the supernatant and coacervate phases $\phi^{\mathrm{I/II}}_{\pm}$ as a function of the asymmetry factor r for the system with $\phi_{p,0} = 0.02$ and $\phi_{s,0} = 0$. Panel (d) denotes the Galvani potential Ψ_G as a function of r.

S3. Concentration profiles, net charge density, and mean electrostatic potential at the interface of asymmetric coacervates with $r = 1/3$ and $\phi_{s,0} = 0$

In Fig. S4, we show the concentration profiles of all charged species along the direction normal to the interface between the supernatant and coacervate phases, for the asymmetric coacervates with different $\phi_{p,0}$ but fixed values of $r = 1/3$ and $\phi_{s,0} = 0$. With increasing $\phi_{p,0}$, the interface broadens gradually. At small $\phi_{p,0}$, the polycation concentration $\phi_{p+}(x)$ exhibits a slight depletion on the supernatant side of the interface, but this depletion van-

ishes completely at large $\phi_{p,0}$ (see Fig. S4(a)). The polyanion concentration $\phi_{p-}(x)$, however, varies monotonically at the interface for all $\phi_{p,0}$ (i.e., Fig. S4(b)). On the other hand, when going from the supernatant to the coacervate phase, the cation concentration $\phi_{+}(x)$ exhibits a slight maximum on the supernatant side of the interface at small $\phi_{p,0}$ and turns to decrease monotonically at large $\phi_{p,0}$. The anion concentration $\phi_{-}(x)$, however, exhibits a maximum on the coacervate side of the interface for all $\phi_{p,0}$, and the value of this maximum becomes less pronounced for larger $\phi_{p,0}$.

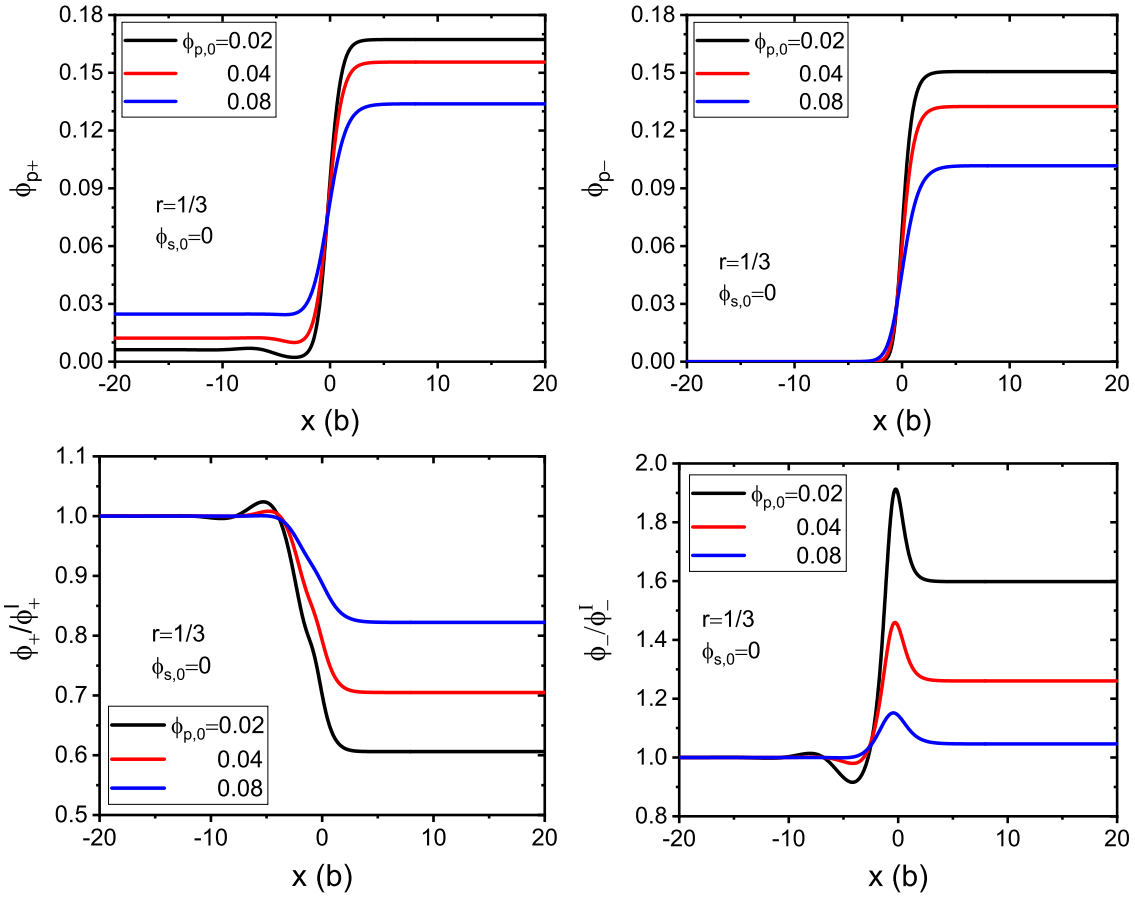

Figure S4: Density profile of (a) polycation, (b) polyanion, (c) small cation, and (d) small anion, for asymmetric coacervates with $r = 1/3$ and $\phi_{s,0} = 0$.

Figs. S5(a) and (b) show the net charge density $\phi_e(x) = \phi_{p+}(x) - \phi_{p-}(x) + \phi_{+}(x) - \phi_{-}(x)$ and the mean electrostatic potential $\psi(x)$, respectively, for the asymmetric coacervates with different $\phi_{p,0}$ and fixed values of $r = 1/3$ and $\phi_{s,0} = 0$. In particular, we observe a strong

oscillation in $\phi_e(x)$ at small $\phi_{p,0}$, and this oscillation becomes weaker with increasing $\phi_{p,0}$. On the other hand, when going from the supernatant to the coacervate phase, $\psi(x)$ at small $\phi_{p,0}$ first decreases slightly and then increases rapidly to Ψ_G after a slight overshoot. For large $\phi_{p,0}$, however, $\psi(x)$ increases monotonically from 0 to Ψ_G.

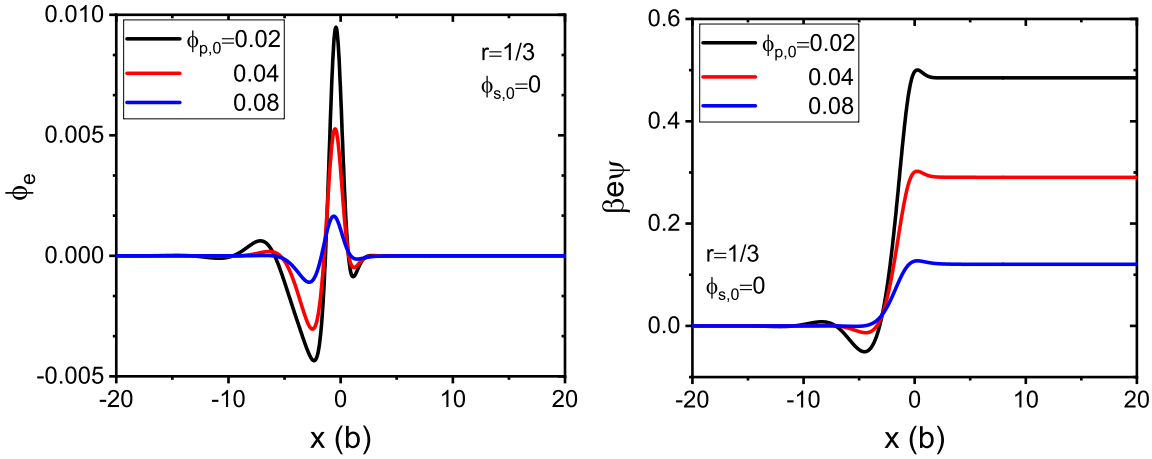

Figure S5: (a) Net charge density ϕ_c and (b) the mean electrostatic potential ψ, for asymmetric coacervates with $r = 1/3$ and $\phi_{s,0} = 0$.

S4. Concentration profiles, net charge density, and mean electrostatic potential at the interface of both symmetric and asymmetric coacervates with $\phi_{p,0} = 0.02$ and $\phi_{s,0} = 0$

In Fig. S6, we show the concentration profiles of all charged species along the direction normal to the interface between the supernatant and coacervate phases, for both symmetric and several asymmetric coacervates with fixed values of $\phi_{p,0} = 0.02$ and $\phi_{s,0} = 0$. Clearly, we see qualitatively different behaviors for the symmetric and asymmetric coacervates. Specifically, the small ion distributions at the interface are quite different for the symmetric and asymmetric coacervates. Moreover, as shown in Fig. S7, while the net charge density $\phi_e(x)$ and the mean electrostatic potential $\psi(x)$ remain identically 0 for the symmetric coacervates, the intricate electric double layer forms spontaneously at the interface. Since the qualita-

tive behaviors for the interface of the asymmetric coacervates have already been discussed previously, they will not be discussed further.

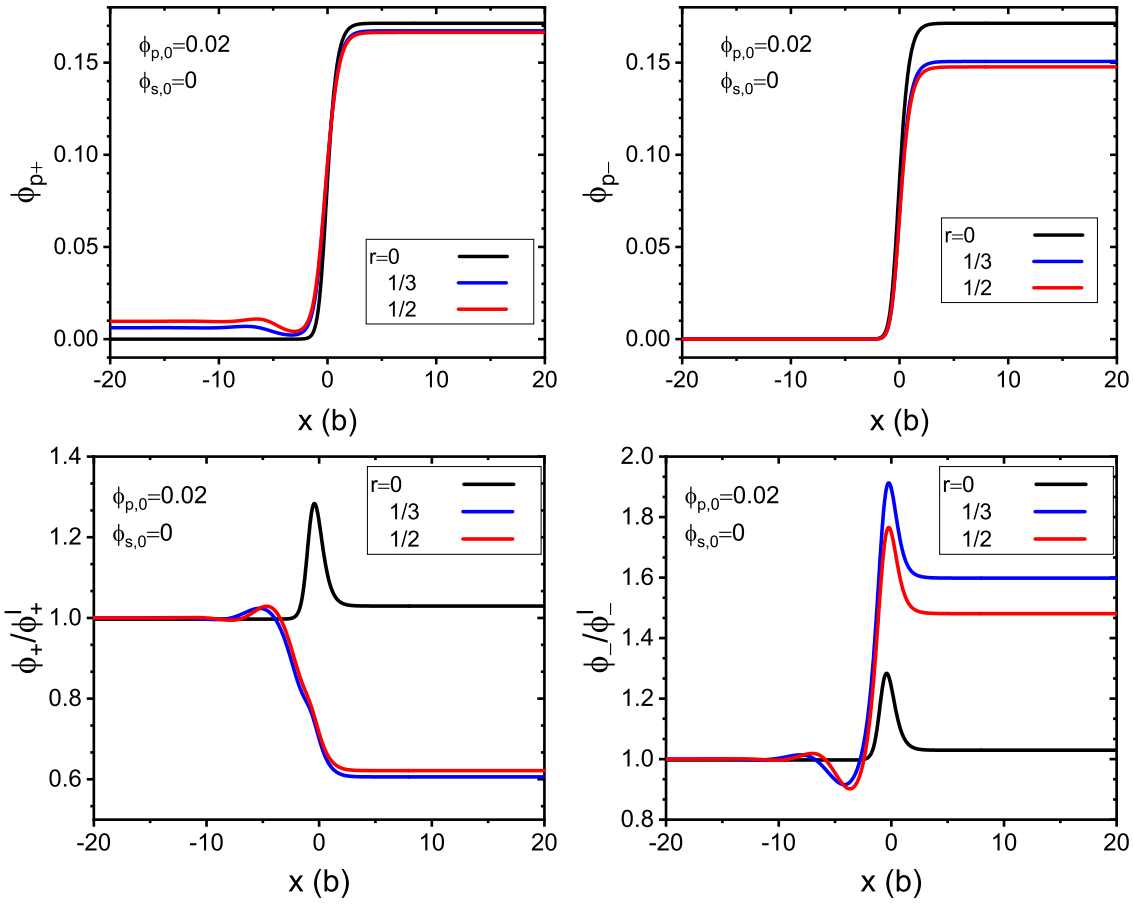

Figure S6: Density profile of (a) polycation, (b) polyanion, (c) small cation, and (d) small anion, for both the symmetric and several asymmetric coacervates with $\phi_{p,0} = 0.02$ and $\phi_{s,0} = 0$.

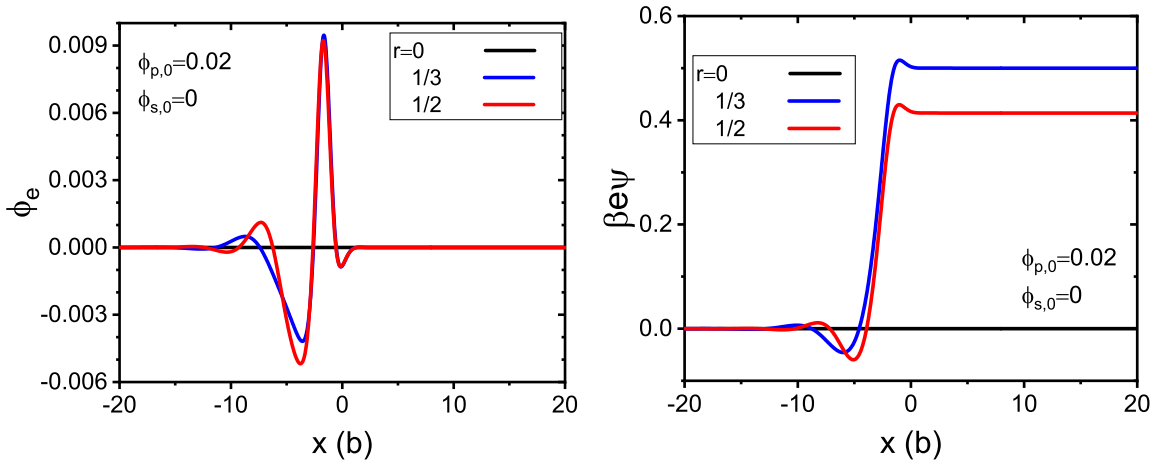

Figure S7: (a) Net charge density ϕ_c and (b) the mean electrostatic potential ψ, for asymmetric coacervates with $\phi_{p,0} = 0.02$ and $\phi_{s,0} = 0$. We also include the curves (i.e., $\phi_c = 0$ and $\psi = 0$ at all x) for the symmetric coacervate as reference.

References

(S1) Zhang, P.; Alsaifi, N. M.; Wu, J.; Wang, Z.-G. Polyelectrolyte Complex Coacervation: Effects of Concentration Asymmetry. *The Journal of Chemical Physics* **2018**, *149*, 163303, DOI: 10.1063/1.5028524.